Tetra-Rhenium Molecular Rectangles as Organizational Motifs for the Investigation of Ligand-Centered Mixed Valency: Three Examples of Full Delocalization

Peter H. Dinolfo and Joseph T. Hupp*

Contribution from the Department of Chemistry, 2145 Sheridan Road, Northwestern University, Evanston, Illinois 60208-3113

Received July 28, 2004; E-mail: jthupp@chem.northwestern.edu

Abstract: Molecular rectangles having the form $\{[Re(CO)_3]_2(X)_2\}_2\text{-}\mu,\mu'\text{-}(LL)_2$, where X is either a bridging alkoxide or phenylthiolate group and LL is 4,4′-bipyridine or pyrazine, are characterized by cofacial LL pairs that are in van der Waals contact across the "long" side of the rectangle. Cyclic voltammetry shows that the redox-accessible bridging ligands, LL, are reduced in sequential, one-electron reactions. The singly reduced rectangles represent an unusual type of mixed-valence compound in which the LL ligands themselves are the redox centers. Spectroelectrochemical measurements for mixed-valence forms of these rectangles reveal intense, asymmetric absorption bands in the near-infrared region, assigned as intervalence transitions. Electroabsorption (Stark spectroscopy) measurements reveal minute changes in dipole moment and therefore a lack of significant charge transfer upon intervalence excitation. Thus, the rectangles are unusual examples of class III (fully valence delocalized) molecular mixed-valence species that employ direct donor-orbital/acceptor-orbital overlap rather than covalent-bond-mediated superexchange to achieve the large electronic coupling strengths required for delocalization.

Introduction

Transition-metal-based coordination chemistry, often coupled with directed-assembly strategies, has proven to be extraordinarily effective for construction of discrete, well-defined supramolecular entities such as squares, triangles, pentagons, and cubes, among others.[1-5] Often the supramolecular structure defines a cavity that can be accessed and occupied by an appropriately sized guest molecule. Advantage has been taken of selective guest encapsulation by transition-metal-based assemblies to demonstrate, for example, both chemical sensing[6-10] and reaction catalysis.[11,12] Also reported has been the use of such structures to facilitate photoinitiated guest-to-host and host-to-guest energy transfer.[13]

We reasoned that certain structures could also be exploited in studies of component-to-component electron transfer, espe-cially degenerate transfer. Particularly interesting from a fundamental perspective could be ligand-to-ligand electron exchange where supramolecular frameworks could spatially configure electron donors and acceptors in fairly precise ways. This could, in turn, allow questions concerning, for example, the effects of (a) intervening, noncovalently bound matter, (b) donor/acceptor separation distance, and (c) donor/acceptor orientation upon exchange rates, electronic coupling energies (H_{ab}), and reorganization energies to be examined in a systematic fashion. Especially instructive concerning the coupling and reorganizational energy parameters would be intervalence absorption spectra (ligand-to-ligand charge-transfer spectra). While numerous examples of metal-based intervalence absorption exist,[14-20] only a small number based on ligands have been reported.[21-26]

(1) Cotton, F. A.; Lin, C.; Murillo, C. A. *Acc. Chem. Res.* **2001**, *34*, 759–771.
(2) Fujita, M. *Chem. Soc. Rev.* **1998**, *27*, 417–425.
(3) Holliday, B. J.; Mirkin, C. A. *Angew. Chem., Int. Ed. Engl.* **2001**, *40*, 2022–2043.
(4) Leininger, S.; Olenyuk, B.; Stang, P. J. *Chem. Rev.* **2000**, *100*, 853–907.
(5) Stang, P. J.; Olenyuk, B. *Acc. Chem. Res.* **1997**, *30*, 502–518.
(6) Sun, S.-S.; Lees, A. J. *J. Am. Chem. Soc.* **2000**, *122*, 8956–8967.
(7) Keefe, M. H.; Slone, R. V.; Hupp, J. T.; Czaplewski, K. F.; Snurr, R. Q.; Stern, C. L. *Langmuir* **2000**, *16*, 3964–3970.
(8) Benkstein, K. D.; Hupp, J. T.; Stern, C. L. *Angew. Chem., Int. Ed. Engl.* **2000**, *39*, 2891–2893.
(9) Chang, S. H.; Chung, K.-B.; Slone, R. V.; Hupp, J. T. *Synth. Met.* **2001**, *117*, 215–217.
(10) Mines, G. A.; Tzeng, B.-C.; Stevenson, K. J.; Li, J.; Hupp, J. T. *Angew. Chem., Int. Ed. Engl.* **2002**, *41*, 154–157.
(11) Merlau, M. L.; Mejia, M. d. P.; Nguyen, S. T.; Hupp, J. T. *Angew. Chem., Int. Ed. Engl.* **2001**, *40*, 4239–4242.
(12) Ito, H.; Kusukawa, T.; Fujita, M. *Chem. Lett.* **2000**, 598–599.
(13) Splan, K. E.; Massari, A. M.; Morris, G. A.; Sun, S.-S.; Reina, E.; Nguyen, S. T.; Hupp, J. T. *Eur. J. Inorg. Chem.* **2003**, 2348–2351.

(14) Creutz, C. *Prog. Inorg. Chem.* **1983**, *30*, 1–73.
(15) Robin, M. B.; Day, P. *Adv. Inorg. Chem. Radiochem.* **1967**, *10*, 247–422.
(16) Crutchley, R. J. *Adv. Inorg. Chem.* **1994**, *41*, 273–325.
(17) Kaim, W.; Klein, A.; Gloeckle, M. *Acc. Chem. Res.* **2000**, *33*, 755–763.
(18) Demadis, K. D.; Hartshorn, C. M.; Meyer, T. J. *Chem. Rev.* **2001**, *101*, 2655–2685.
(19) Ito, T.; Hamaguchi, T.; Nagino, H.; Yamaguchi, T.; Kido, H.; Zavarine, I. S.; Richmond, T.; Washington, J.; Kubiak, C. P. *J. Am. Chem. Soc.* **1999**, *121*, 4625–4632.
(20) Elliott, C. M.; Derr, D. L.; Matyushov, D. V.; Newton, M. D. *J. Am. Chem. Soc.* **1998**, *120*, 11714–11726.
(21) Heath, G. A.; Yellowlees, L. J.; Braterman, P. S. *Chem. Phys. Lett.* **1982**, *92*, 646–648.
(22) Coombe, V. T.; Heath, G. A.; MacKenzie, A. J.; Yellowlees, L. J. *Inorg. Chem.* **1984**, *23*, 3423–3425.
(23) Chang, H.-C.; Kitagawa, S. *Angew. Chem., Int. Ed. Engl.* **2002**, *41*, 130–133.
(24) Chang, H.-C.; Mochizuki, K.; Kitagawa, S. *Inorg. Chem.* **2002**, *41*, 4444–4452.
(25) Chang, H.-C.; Miyasaka, H.; Kitagawa, S. *Inorg. Chem.* **2001**, *40*, 146–156.

Molecular rectangles featuring metal-ion corners comprise one motif well suited to ligand-to-ligand charge-transfer studies. Compounds such as the bis-benzimidazolate (short side)/LL (long side, where LL is a linear dipyridyl ligand such as pyrazine or 4,4′-bipyridine) assembly, **1**, can reversibly take up as many as four electrons, storing them in the longer ligands. When reduced by an odd number of electrons, molecules such as **1** are ligand-based mixed-valence systems. We reported elsewhere on the mixed-valence characteristics of a series of compounds related to both **1**$^{1-}$ and **1**$^{3-}$.[27] Briefly, the compounds are characterized by substantially greater than van der Waals ligand/ligand separation distances, at least at ligand termini, and electronic coupling behavior ranging from nearly class I (fully isolated, noninteracting, valence-localized donor and acceptor sites) to strongly class II (very substantially coupled but still valence localized).
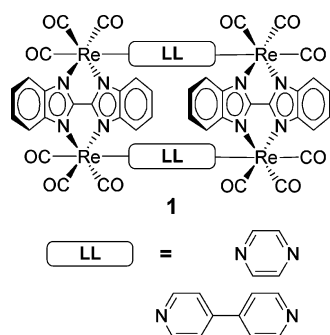
We reasoned that if rectangles featuring shorter "short sides" were examined in mixed-valence form, the resulting enhanced donor-orbital/acceptor-orbital overlap might engender extremely strong electronic coupling, culminating in fully delocalized (class III) behavior. Systematic absorbance and electroabsorbance studies of rectangles **2**−**4** in singly reduced form show that this is indeed the case.
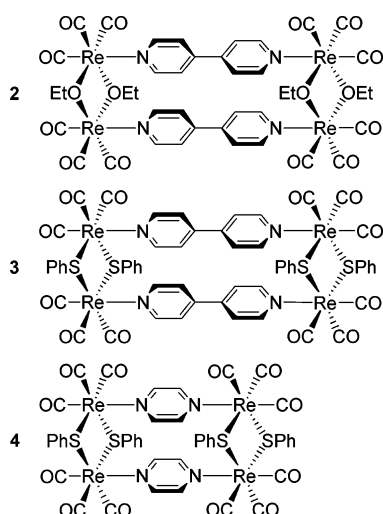
Results

Rectangle Synthesis and Structures. 2 was obtained by the method of Woessner and Sullivan, a convenient single-pot synthesis that recruits deprotonated alcohol solvent molecules

(26) Pratt, R. C.; Stack, T. D. P. *J. Am. Chem. Soc.* **2003**, *125*, 8716−8717.
(27) Dinolfo, P. H.; Williams, M. E.; Stern, C. L.; Hupp, J. T. *J. Am. Chem. Soc.* **2004**, *126*, 12989−13001.

Table 1. Reduction Potentials (V vs Fc/Fc$^+$)

rectangle	$E^{0/1-}_{1/2}$	$E^{1-/2-}_{1/2}$	$E^{2-/4-}_{1/2}{}^a$	$\Delta E^{0/1-/2-}$	$K_c{}^b$	solvent^c
2	−1.59	−1.82		0.23	7.7×10^3	THF
3	−1.54	−1.77	−2.60	0.23	7.7×10^3	THF
4	−1.23	−1.67		0.44	2.7×10^7	THF

^{a} 2−/3− and 3−/4− voltammetric waves strongly overlap. ^{b} Mixed-valence ion (1−) comproportionation constant. ^{c} 0.1 M TBAPF$_6$ used as supporting electrolyte.
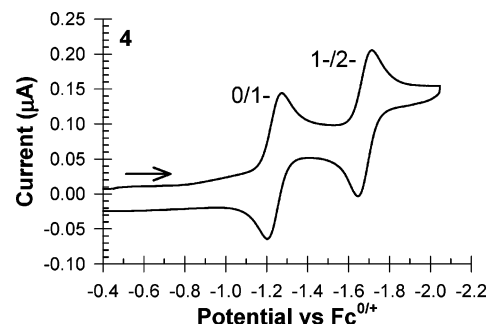

Figure 1. Cyclic voltammogram of **4** in THF with 0.1 M TBAPF$_6$ as the supporting electrolyte.

as bridging alkoxide ligands.[28] Notably, Woessner and Sullivan also reported a single-crystal X-ray structure of the methoxo version of **2**. Their structure is characterized by Re−Re distances of 3.4 Å on the short sides of the rectangle and an average bipyridine/bipyridine spacing of ca. 3.6 Å. In addition to mandating full van der Waals contact between the bipyridine ligands, the tight metal framework enforces a planar ligand conformation, i.e., a dihedral angle of just 9°. We were unsuccessful in extending the synthesis to pyrazine-containing compounds. Therefore, the pyrazine rectangle and a second bipyridine rectangle, **3** and **4**, were instead prepared as *μ*-thiolate compounds using Benkstein's stepwise synthesis.[29] The phenyl thiolate derivatives were chosen, in lieu of alkanethiolates, due to the enhanced solubility properties required for electroabsorbance studies and the relative synthetic ease with which the required di-rhenium intermediate[30] could be obtained. Returning to Benkstein's alkanethiolate versions of **3** and **4**, he likewise reported single-crystal X-ray structures. The salient features are Re−Re separation distances of 3.8 Å for both, average long-edge ligand/ligand spacings of 3.7 Å for both, full van der Waals contact for the long-edge ligands of both, and an essentially planar bipyridine conformation (dihedral angle of 2°).

Electrochemistry and Spectroelectrochemistry. The minor changes in bridging alkoxide and thiolate ligand composition elicit almost no change in reduction potentials for **2**−**4** versus those of the previously reported rectangles. The first two reductions in each instance are one-electron events, and the formal potential differences (Table 1; Figure 1) are sufficient to permit both chemical and electrochemical preparation of solutions containing greater than 98% of each rectangle in the 1− mixed-valent form. The next reduction, in each case, appears to be a two-electron process by cyclic voltammetry but likely is two closely spaced one-electron reductions.

As noted above and corroborated by visible-region spectroelectrochemical (SEC) measurements, the accessible reductions
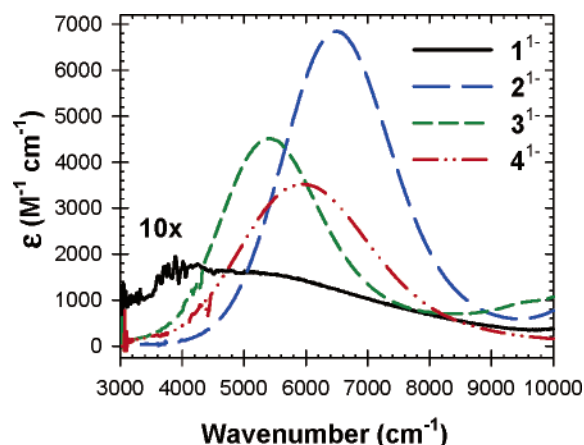
(28) Woessner, S. M.; Helms, J. B.; Shen, Y.; Sullivan, B. P. *Inorg. Chem.* **1998**, *37*, 5406−5407.
(29) Benkstein, K. D.; Hupp, J. T.; Stern, C. L. *Inorg. Chem.* **1998**, *37*, 5404−5405.
(30) Lee, K. W.; Brown, T. L. *Inorg. Chem.* **1987**, *26*, 1852−1856.

Table 2. IT Band Absorption Data

| rectangle	ν_{max} (cm^{-1})	ϵ (M^{-1} cm^{-1})	$\Delta\nu_{1/2}$ (cm^{-1})
2^{1-}	6500	6800	2050
3^{1-}	5600	4550	2125
4^{1-}	5880	4100	2480

Figure 2. IT absorption bands of the pyrazine version of **1**$^{1-}$ (solid black line, shown at 10× intensity), **2**$^{1-}$ (long dashed blue line), **3**$^{1-}$ (short dashed green line), and **4**$^{1-}$ (dashed–dotted red line) in THF.

involve the 4,4′-bipyridine and pyrazine ligands. Thus, the first reduction of **2** is accompanied by absorption bands at ca. 460, 590, and 650 nm, characteristic of the radical anion form of 4,4′-bipyridine. Nearly identical behavior is seen for **3**. For both **2** and **3**, further reduction to the 2− state causes the band intensities to increase.

A slightly different pattern is seen for **4**. A weak band at 456 nm, assigned as a rhenium-to-pyrazine charge-transfer band, decreases in intensity upon reduction to the 1− state and disappears when fully reduced to the 2− state. Coinciding with the reduction from 0 to 2− and the diminution of the band at 456 nm is the growth of a weak band at 700 nm assigned as a pyrazine anion-localized transition.

Extension of the SEC measurements into the near-infrared region reveals low-energy bands for the 1− forms of **2**, **3**, and **4**. The bands, which are absent for both the neutral and doubly reduced versions of the rectangles, are assigned as intervalence transitions (IT). Table 2 contains quantitative IT band absorption data for **2**$^{1-}$, **3**$^{1-}$, and **4**$^{1-}$. A comparison (Figure 2) with the intervalence absorption spectrum of the pyrazine version of **1**$^{1-}$ (shown at 10× intensity), a class II compound, shows that the NIR absorptions for **2**–**4** are significantly narrower and higher in intensity. Both changes tend to be hallmarks of increased electronic coupling—a reasonable interpretation given the greater ligand/ligand contact achievable with the alkoxide- and thiolate-bridged compounds. Whether the coupling strengths are high enough to induce class III (fully delocalized) behavior is a question examined in the next section.

Electroabsorbance Spectroscopy and Mixed-Valence Analysis. Electroabsorbance or Stark spectroscopy reports on changes in molecular polarizability and changes in dipole moment upon optical excitation. Stark spectra are difference spectra obtained by measuring sample absorbances in the presence and absence of an external electric field. Stark signals scale as the field-strength squared. Fields in excess of 10^6 V/m are typically required in order to obtain reasonable signal-to-noise ratios. Our
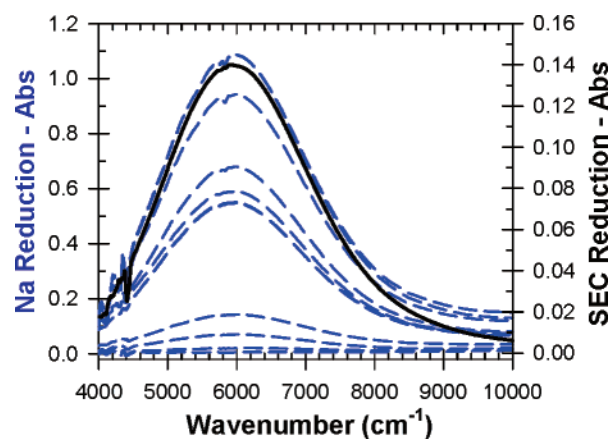
Figure 3. NIR absorption spectra obtained during the reaction of **4** with 5% NaHg, in butyronitrile, in the presence of [2.2.2]-cryptand (dashed blue lines) and absorption obtained during an SEC experiment in THF (solid black line). The chemical reduction is performed at a significantly higher concentration to obtain adequate samples for analysis by Stark.

instrumentation applies voltages of no greater than ∼4000 V, meaning that short optical path lengths are needed. A typical path length is 50 μm. Additionally, to prevent sample molecule migration and reorientation in response to the field, the measurement is performed in a rigid matrix. Here, 77 K solvent glasses were used. Finally, large absorbances (ideally ca. 0.3–0.6), and therefore high sample concentrations, are desirable. Incorporation of modified alkoxide and thiolate ligands in **2**–**4**, as described above, proved essential in this regard.

To obtain high-quality glasses and comparatively high mixed-valence ion concentrations, we found chemical reduction with sodium–mercury amalgam to be superior to electrochemical reduction with the best results generally obtained in the presence of [2.2.2]-cryptand, a sodium-ion complexing agent. Among other effects we reasoned that the complexing agent would minimize ion pairing, a factor known to be important in the intervalence spectroscopy of some compounds.[31] Figure 3, a progressive reduction of **4** with 5% sodium–amalgam, illustrates the straightforward nature of mixed-valence ion formation in this fashion (dashed blue lines). Included for comparison is the electrochemically generated intervalence spectrum (solid black line). Notably, samples prepared chemically were considerably more stable, lasting several hours at ambient temperature in the absence of air and moisture.

Figure 4 shows the Stark response of **2**$^{1-}$ in butyronitrile at 77 K at four field strengths at an angle of 55°. As shown in the inset, the signal intensity exhibits the expected field-squared dependence.

Figure 5 presents a quantitative Liptay analysis of the Stark response of another of the rectangles, **4**$^{1-}$. The top panel (a) shows the unperturbed absorption spectra at 77 K in butyronitrile, and panel b shows its energy-weighted first (dashed blue line) and second (dashed green line) derivatives. Panels c and d contain experimental Stark spectra (solid black line) collected at $\chi = 90°$ and 55°, respectively. Also plotted on graph c and d are the zero-, first-, and second-derivative components of the fit to the Stark signal (open circles). Most notable is the lack of a strong second-derivative (dashed green line) component to the Stark signal. This indicates the absence of a significant dipole

(31) Blackbourn, R. L.; Dong, Y.; Lyon, L. A.; Hupp, J. T. *Inorg. Chem.* **1994**, *33*, 4446–4452.
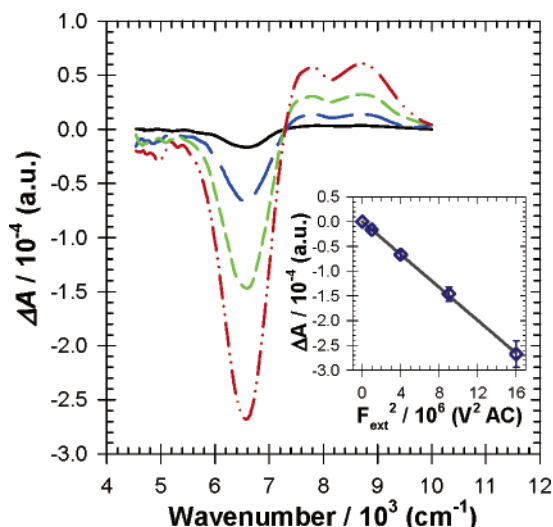
Figure 4. NIR Stark response for 2^{1-} in butyronitrile at 77 K ($\chi = 55°$), shown at four different field strengths: $F_{ext} = 1$ (solid black line), 2 (long dashed blue line), 3 (short dashed green line), and 4 kV (dashed–dotted red line). The inset graph shows the Stark response (blue diamonds) at 6500 cm^{-1} as a function of F_{ext}^2 with the linear regression (black line).

change, $\Delta\mu_{12}$, upon intervalence excitation. Equivalently, it indicates a near-zero adiabatic charge-transfer distance R_{12}, where

$$eR_{12} = \Delta\mu_{12} \qquad (1)$$

and e is the unit electronic charge; see Table 3. In other words, the reduced rectangle behaves as a class III mixed-valence system.

Returning to Figure 5, the largest contributors to the Stark spectrum are the unperturbed absorption spectrum and the first-derivative component. Quantifying the analysis at the two measured angles, contributions from the B-term correspond to $\Delta\alpha = -39$ Å^3 and $Tr\Delta\alpha = -48$ Å^3. While not often encountered, negative polarizability changes are, in fact, expected in the two-state limit (i.e., the ground state and a single electronic excited state).[32,33] Positive values arise when significant upper-excited-state configuration interactions exist. For mixed-valence systems, superexchange coupling of initial and final states is one way in which upper-excited-state involvement can be of chemical significance. We interpret the negative polarizability changes observed here as evidence that electronic coupling and valence delocalization in 4^{1-} is achieved mainly through direct donor-orbital/acceptor-orbital overlap rather than through superexchange interactions involving the coordinated metal centers and bridging thiolates.

Included as Supporting Information are Stark spectra and analyses for rectangles 2^{1-} and 3^{1-}. As illustrated by the polarizability change and charge-transfer distance data in Table 3, these behave similarly to 4^{1-} and clearly also are valence delocalized. In the class III limit, a particularly simple relation exists between the intervalence band maximum and the electronic coupling energy

$$H_{ab} = v_{max}/2 \qquad (2)$$

The H_{ab} values obtained are substantial: 3250, 2800, and 2940 cm^{-1} for 2^{1-}, 3^{1-}, and 4^{1-}, respectively. The slightly larger value for 2^{1-} in comparison to 3^{1-} and 4^{1-} is consistent with
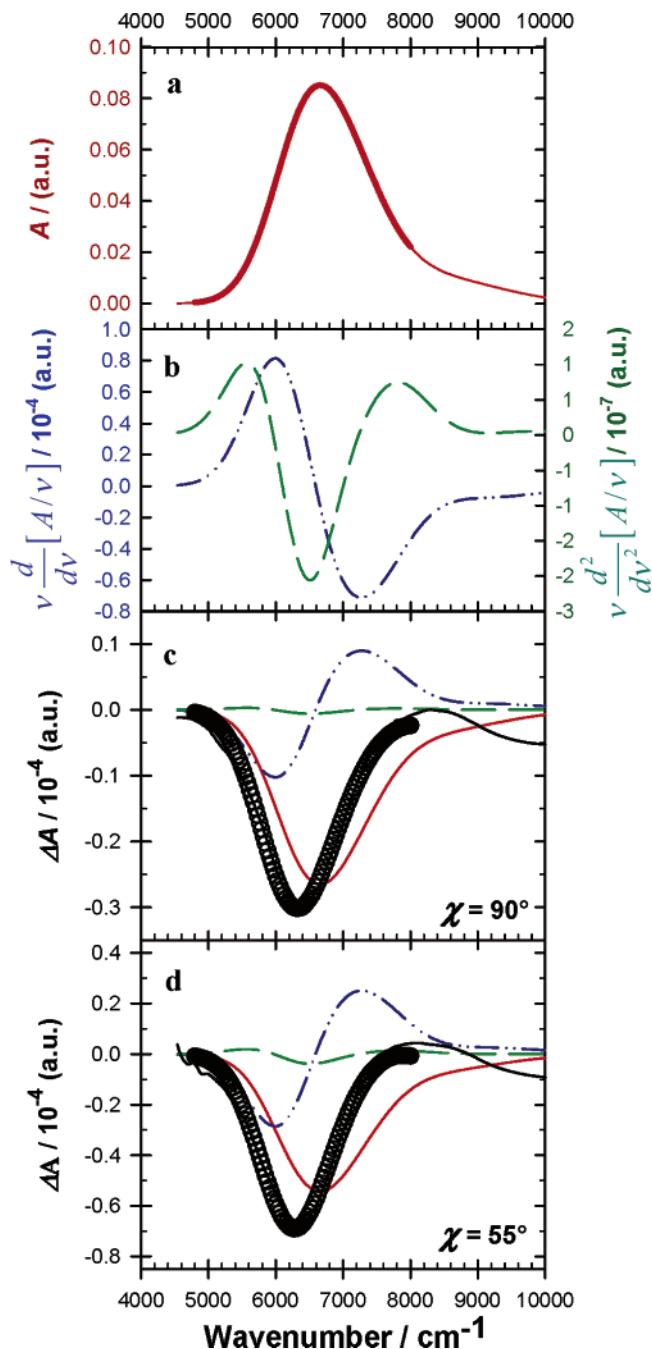

Figure 5. Liptay analysis of the Stark spectra for 4^{1-}. (a) Unperturbed absorption specta at 77 K in butyronitrile (solid red line), and (b) energy-weighted first and second derivatives (dashed–dotted blue line and dashed green line, respectively). (c and d) Measured (solid black lines) and fit (open circles) Stark signals at $\chi = 90°$ and 55°, respectively. Included with the fits are the contributions from the absorption spectra (red) and the first and second derivatives (dashed–dotted blue line and dashed green line, respectively).

the shorter ligand/ligand spacing and presumably greater orbital overlap enforced by the rhenium–ethoxo fragments (with the tighter rhenium spacing in the ethoxo case reflecting the smaller size of oxygen versus sulfur as a bridging atom). Also favoring effective orbital overlap is the highly symmetrical donor-ligand/ acceptor-ligand geometry. Typically observed, but absent here,

(32) Meyers, F.; Marder, S. R.; Pierce, B. M.; Bredas, J. L. *J. Am. Chem. Soc.* **1994**, *116*, 10703–10714.
(33) Shin, Y. K.; Brunschwig, B. S.; Creutz, C.; Sutin, N. *J. Phys. Chem.* **1996**, *100*, 8157–8169.

Table 3. Stark Absorption (IT band) Data[a]

compound	$|\Delta\mu_v|^b$ (e·Å)	ξ^c(°)	$Tr\Delta\alpha^d$ (Å³)	$\Delta\alpha^e$ (Å³)
2[1−]	0.14 ± 0.01	0	−46 ± 0.2	−52 ± 1.0
3[1−]	0.20 ± 0.02	0	−51 ± 0.6	−63 ± 2.4
4[1−]	0.15 ± 0.01	0	−39 ± 4.5	−48 ± 12

[a] Butyronitrile solutions, 77 K. [b] Vector dipole moment change. [c] Angle between the transition dipole moment and the $\Delta\mu_{\varpi}$ vector. [d] Trace of the polarizability change. [e] Polarizability change along the transition moment.

is lateral slippage such that cofacial units place hydrogen atoms from one set of aromatic rings over the centers of the opposing rings. Evidently the demands imposed by supramolecular coordination are sufficient to cancel the electrostatic (π stacking) advantages anticipated for slipped configurations.

Conclusions

One-electron reduction of molecular rectangles featuring pyrazine or bipyridine ligands along the long sides and μ-alkoxides or μ-phenylthiolates along the short sides produces ligand-centered mixed-valence compounds. The ligand/ligand van der Waals contact enforced by the rectangle motif leads to strong electronic coupling, as evidenced by intense intervalence transitions in the near-infrared region. Intervalence Stark spectroscopy shows that the coupling is sufficiently great to induce full valence delocalization. The Stark measurements also suggest that coupling is dominated by direct, noncovalent donor-orbital/acceptor-orbital overlap rather than by superexchange coupling through the rectangle framework.

Experimental Section

General Methods. Infrared spectra were recorded on a Bio-Rad FTS-40 FTIR spectrometer. All NMR spectra were recorded on either a Varian Mercury-400 MHz or a Varian INOVA-500 MHz spectrometer, and the chemical shifts were referenced to the standard solvent shift. FAB LRMS and HRMS were performed at the Michigan State University Mass Spectrometry Facility using a JEOL HX-110 double-focusing mass spectrometer. Elemental analyses were performed by Atlantic Microlabs, Inc., Norcross, GA. UV−vis−NIR absorption spectra were measured using a Varian Cary 5000 spectrometer.

Materials. All commercial reagents were of ACS grade and used without further purification. Tetrahydrofuran (THF) was purified using a two-column solid-state purification system (Glasscontour System, Joerg Meyer, Irvine, CA). 4,4′-Bipyridine, pyrazine, phenyl disulfide, and rhenium decacarbonyl were purchased from Aldrich and used without further purification. [Re(CO)$_4$]$_2$(SPh)$_2$[30] and **2**[28] were synthesized via literature methods. Butyronitrile was purchase from Aldrich and stored over 4 Å molecular sieves.

General Rectangle Synthesis. 3 and **4** were synthesized by the method of Benkstein.[29] Briefly, stoichiometric amounts of [Re(CO)$_4$]$_2$-(SPh)$_2$ and the bridging ligand, 4,4′-bipyridine or pyrazine, were refluxed together in CHCl$_3$ for 2 days. Following recrystallization from THF and hexanes, the pure rectangles were collected by filtration.

([Re(CO)$_3$]$_2$(SPh)$_2$)$_2$-μ,μ'-(4,4′-bipyridine)$_2$ (3). [Re(CO)$_4$]$_2$(SPh)$_2$ (53 mg, 0.065 mmol) and 4,4′-bipyridine (10.2 mg, 0.065 mmol) yielded 43 mg of **3** as an orange powder (72% yield). IR (THF, cm^{-1}) 2025 (C≡O), 2012 (C≡O), 1929 (C≡O), 1904 (C≡O). ^{1}H NMR (500 MHz, THF-d_8) δ 9.30 (d, 8H), 7.89 (d, 8H), 7.71 (d, 8H), 7.39 (t, 8H), 7.21 (t, 4H). LRMS−FAB (*m/z*): [M$^+$] calcd, 1829.9; found, 1829.8. Anal. Calcd for Re$_4$C$_{56}$H$_{36}$N$_4$O$_{12}$S$_4$: C, 36.75; H, 1.98; N, 3.06; S, 7.01. Found: C, 36.51; H, 2.27; N, 3.15; S, 6.82.

([Re(CO)$_3$]$_2$(SPh)$_2$)$_2$-μ,μ'-(pyrazine)$_2$ (4). [Re(CO)$_4$]$_2$(SPh)$_2$ (60 mg, 0.07 mmol) and pyrazine (8.5 mg, 0.07 mmol) yielded 50 mg of **4** as an orange powder (81% yield). IR (THF, cm^{-1}) 2026 (C≡O), 2017

(C≡O), 1937 (C≡O), 1916 (C≡O). ^{1}H NMR (500 MHz, THF-d_8) δ 9.33 (s, 8H), 7.86 (d, 8H), 7.41 (t, 8H), 7.25 (t, 4H). LRMS−FAB (*m/z*): [M$^+$] calcd, 1677.8; found, 1677.8. HRMS−FAB (*m/z*): [M$^+$] calcd for ^{187}Re$_3$^{185}ReC$_{44}$H$_{28}$N$_4$O$_{12}$S$_4$, 1677.8788; found, 1677.8790(6). Anal. Calcd for Re$_4$C$_{44}$H$_{28}$N$_4$O$_{12}$S$_4$·(THF): C, 32.88; H, 2.07; N, 3.20; S, 7.30. Found: C, 32.40; H, 2.18; N, 3.34; S, 7.39.

Electrochemistry. All cyclic voltammetric experiments were performed and analyzed using a CHI900 (CH Instruments, Austin, TX) potentiostat. Electrolyte solutions (0.1 M tetrabutylammonium hexafluorophosphate (TBAPF$_6$) (>99%, Fluka)) were prepared with anhydrous solvents and nitrogen degassed before use. A Pt wire was used as the counter electrode, and 2 mm diameter Pt or Au macro disk electrodes were used as the working electrodes. A silver wire was used as a pseudo-reference electrode with ferrocene (Aldrich, purified by sublimation) added as an internal reference at the end of each experiment. All experiments were run under an N$_2$ atmosphere.

Spectroelectrochemistry. UV−vis−NIR spectroelectrochemistry (SEC) experiments were performed with a previously described cell[27] using a Varian CARY 5000 spectrometer and a Princeton Applied Research model 273 potentiostat. [NBu$_4$][B(C$_6$F$_5$)$_4$][34] (0.02 M) was used as the supporting electrolyte because the high conductivity allowed lower concentrations to be used, improving background subtractions in near-infrared (NIR) spectral measurements.

Electroabsorption Spectroscopy (Electronic Stark Effect Spectroscopy). All samples were prepared under a dry nitrogen atmosphere (benchtop glovebag). Typically, 5 mg of a rectangle sample were added to 1−2 mL of butyronitrile or butyronitrile−THF mixtures with 10 mg of [2.2.2]-cryptand in a 1 mm quartz cuvette with a Teflon screw-top. The samples were then reduced with 5% NaHg while monitoring their UV−vis−NIR absorbance. Once the near-infrared absorbance had been maximized, the sample solutions were filtered through a 0.22 μm Teflon filter and transferred to the Stark apparatus.

Stark absorption measurements were conducted in a fashion similar to previous reports[35] but with modifications as follows: Experiments were conducted in a dual liquid nitrogen immersion cryostat (Janis Research Corporation) at 77 K.[36] The sample solutions were placed between two indium−tin oxide (ITO) coated quartz slides (Delta Technologies, ITO thickness ca. 2000 Å) separated by 50 μm Kapton spacers (DuPont). The electrodes were baked at 450 °C for approximately 2 h to increase their transmittance in the NIR. No difference of AC field stability was seen in Stark experiments with baked versus unbaked electrodes. The same electrodes were used for all experiments. The path length of the cell was confirmed interferometrically by measuring interference patterns in the near-infrared region with the empty cell.

The experimental electroabsorbance setup is similar to that previously described[35] but with several modifications to extend and improve the response in the near-infrared region. The light from a 90-W tungsten−halogen lamp, with a DC-regulated power supply (PTI), was sent through the monochromator of an OLIS modified Cary-14 spectrometer. The exiting light was horizontally polarized using an α-BBO Glan-Taylor prism (U−Oplaz Technologies), focused through the sample cryostat using CaF$_2$ lenses (Janos Technologies), and detected with a photovoltaic HgCdTe detector that was thermoelectrically cooled to −40 °C (Judson Technologies). With this detector the instrument has a working wavelength range of 800−2600 nm. The typical spectral bandwidth ranged from 4 to 10 nm over the scanned wavelength ranges. No significant changes were observed for smaller bandwidths.

Stark Absorption Analysis. Analysis of the data was performed using the Liptay method[37,38] as described in detail elsewhere[35] and only

(34) LeSuer, R. J.; Geiger, W. E. *Angew. Chem., Int. Ed. Engl.* **2000**, *39*, 248−250.
(35) Karki, L.; Hupp, J. T. *Inorg. Chem.* **1997**, *36*, 3318−3321.
(36) Andrews, S. S.; Boxer, S. G. *Rev. Sci. Instrum.* **2000**, *71*, 3567−3569.
(37) Liptay, W. *Angew. Chem., Int. Ed. Engl.* **1969**, *8*, 177−188.
(38) Liptay, W. In *Excited States*; 1974; Vol. 1, pp 129−229.

briefly summarized here. Each Stark spectrum was fit to a linear combination of the zero, first, and second derivatives of the low-temperature absorption spectrum $A(v)$

$$\Delta A(v) = \left\{ A_\chi A(v) + \frac{B_\chi v}{15hc} \frac{d[A(v)/v]}{dv} + \frac{C_\chi v}{30h^2c^2} \frac{d^2[A(v)/v]}{dv^2} \right\} F_{int}^2 \quad (3)$$

In eq 3, $\Delta A(v)$ is the frequency-dependent absorption change resulting from electric field modulation, h is Planck's constant, c is the speed of light in a vacuum, and v is the frequency of the absorbed light. F_{int} is the internal electric field experienced by the chromophore and can be written as

$$F_{int} = f F_{ext} \quad (4)$$

where F_{ext} is the externally applied electric field and f is the local-field correction. $f = 1.3$, a value typically used for organic solvents,[39] was assumed for all calculations. It should be noted, however, that uncertainties of perhaps 20% exist for f. The coefficients A_χ, B_χ, and C_χ provide information about electric-field-induced changes in the transition dipole moment and about excited-state/ground-state polar-

(39) Bublitz, G. U.; Boxer, S. G. *Annu. Rev. Phys. Chem.* **1997**, *48*, 213−242.

izability and dipole moment differences, respectively. The molecular parameters are determined as follows

$$A_\chi = \frac{\langle \alpha_m \rangle}{3} + (^1/_{30})(3 \cos^2 \chi - 1)[3\langle \beta_m \rangle - 2\langle \alpha_m \rangle] \quad (5)$$

$$B_\chi = (5/2)Tr\Delta\alpha + (3 \cos^2 \chi - 1)((3/2)\hat{g}\Delta\alpha\hat{g} - (^1/_2)Tr\Delta\alpha) \quad (6)$$

$$C_\chi = |\Delta\mu_v|^2[5 + (3 \cos^2 \xi - 1)(3 \cos^2 \chi - 1)] \quad (7)$$

In these equations, $\langle \alpha_m \rangle$ and $\langle \beta_m \rangle$ are the scalar portions of the transition moment polarizability and hyperpolarizability tensors, $Tr\Delta\alpha$ is the trace of the polarizability difference between the excited and ground electronic states, $\hat{g}\Delta\alpha\hat{g}$ is the polarizability change along the transition moment ($\hat{g}$ is the unit vector), $\Delta\mu_v$ is the vector change in dipole moment, χ is the angle between the light and electric field vectors, and ξ is the angle between transition dipole moment and $\Delta\mu_v$ vectors.

Supporting Information Available: UV−vis absorption spectra for **2**, **3**, and **4** in the 0, 1−, and 2− states. NIR Stark spectra and Liptay analyses for rectangles $\mathbf{2^{1-}}$ and $\mathbf{3^{1-}}$. This material is available free of charge via the Internet at http://pubs.acs.org.

JA045457D